

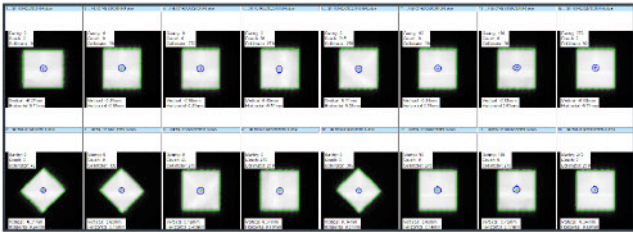
OPTIMIZE YOUR SRS/SBRT QA

WITH SUB-MILLIMETER ACCURACY

ISOCENTER OPTIMIZATION ROUTINE



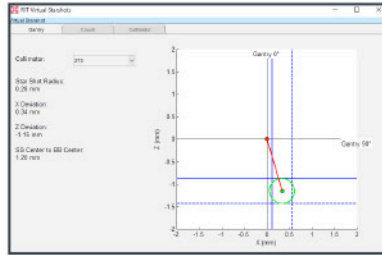
Utilize RIT software's 3D Winston-Lutz Isocenter Optimization routine for a fast and precise measurement of isocenter accuracy, now with added support for Elekta Unity machines. Using only a set of EPID Winston-Lutz images, the RIT system will calculate deviations between radiation and mechanical isocenter, determine ball/BB setup error, and suggest couch alignment adjustments to maximize your system's accuracy.



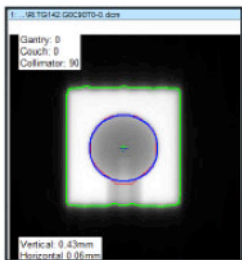
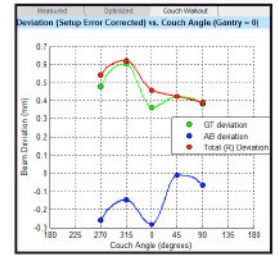
Automatically process a range of 3 to 16 EPID Winston-Lutz images for fast, sub-millimeter level accuracy of isocenter position. The routine allows physicists to perform daily or patient-specific analyses using specific clinical treatment angles with a ball setup error reported for each test. In addition to performing a full system analysis, you can perform partial system analyses and generate results with as few as 3 images.

Eliminate your need for films and increase your accuracy using RIT's patented Virtual Star Shot feature with any combination of angles, reconstructed using a set of Winston-Lutz images in its dedicated window.

Patents: US 9192784, JP 6009705, CA 2918045, and other international patents pending.



The Couch Walkout Plot displays beam deviation vs. couch rotation angle, which is a significant enhancement for customers adjusting the couch angle.



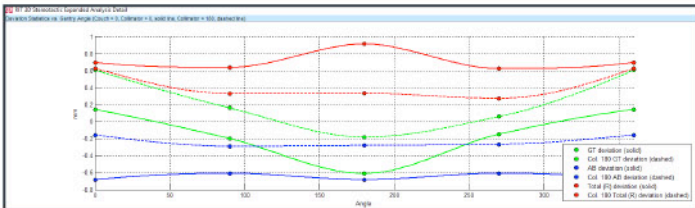
RIT's Isocenter Optimization routine allows for optimal cone detection, resulting in sub-pixel precision.

Maximum Deviation:

- 1.01 mm (measured, setup error included)
- 0.78 mm (setup error corrected)
- 0.52 mm (Maximum Measured Deviation with Setup Error Removed (R))

The measured deviation with setup error corrected (R) is with the ball setup at gantry isocenter. It is the Euclidean distance of the individual GT and AB components. The reported maximum deviation can be found in the "Measured" tab, where it is the maximum value under the R column.

Information icons present clear and easy annotations to guide you through the advanced analysis. Users can choose to pass or fail on the Maximum Machine Deviation (R) or the Total Maximum Deviation (W), which includes the ball setup error.



The routine enables individual component (gantry, collimator, couch) characterization to better understand distinct contributions to isocenter deviation, giving insight into adjustments that can be made to improve delivery performance, if needed.

CLICK TO VISIT RADIMAGE.COM TODAY TO DEMO THIS ADVANCED QA ROUTINE FROM RADIOLOGICAL IMAGING TECHNOLOGY, INC.



+1 (719) 590-1077, OPT. 4

SALES@RADIMAGE.COM

Connect with us on social media



Fully automated measurement of intracranial CSF and brain parenchyma volumes in pediatric hydrocephalus by segmentation of clinical MRI studies

Carmela Russo¹ | Maria Agnese Pirozzi^{2,3}  | Federica Mazio¹ |
 Daniele Cascone¹ | Domenico Cicala¹ | Maria De Liso¹ | Anna Nastro¹ |
 Eugenio Maria Covelli¹ | Giuseppe Cinalli⁴ | Mario Quarantelli² 

¹Neuroradiology Unit, Department of Neuroscience, Santobono-Pausilipon Children's Hospital, Naples, Italy

²Institute of Biostructures and Bioimaging, National Research Council, Naples, Italy

³Department of Advanced Medical and Surgical Sciences, University of Campania "Luigi Vanvitelli", Naples, Italy

⁴Pediatric Neurosurgery Unit, Department of Neuroscience, Santobono-Pausilipon Children's Hospital, Naples, Italy

Correspondence

Maria Agnese Pirozzi, Institute of Biostructures and Bioimaging, National Research Council, Naples, Italy.
 Email: mariaagnese.pirozzi@ibb.cnr.it

Abstract

Background: Brain parenchyma (BP) and intracranial cerebrospinal fluid (iCSF) volumes measured by fully automated segmentation of clinical brain MRI studies may be useful for the diagnosis and follow-up of pediatric hydrocephalus. However, previously published segmentation techniques either rely on dedicated sequences, not routinely used in clinical practice, or on spatial normalization, which has limited accuracy when severe brain distortions, such as in hydrocephalic patients, are present.

Purpose: We developed a fully automated method to measure BP and iCSF volumes from clinical brain MRI studies of pediatric hydrocephalus patients, exploiting the complementary information contained in T2- and T1-weighted images commonly used in clinical practice.

Methods: The proposed procedure, following skull-stripping of the combined volumes, performed using a multiparametric method to obtain a reliable definition of the inner skull profile, maximizes the CSF-to-parenchyma contrast by dividing the T2w- by the T1w- volume after full-scale dynamic rescaling, thus allowing separation of iCSF and BP through a simple thresholding routine.

Results: Validation against manual tracing on 23 studies (four controls and 19 hydrocephalic patients) showed excellent concordance (ICC > 0.98) and spatial overlap (Dice coefficients ranging from 77.2% for iCSF to 96.8% for intracranial volume). Accuracy was comparable to the intra-operator reproducibility of manual segmentation, as measured in 14 studies processed twice by the same experienced neuroradiologist. Results of the application of the algorithm to a dataset of 63 controls and 57 hydrocephalic patients (19 with parenchymal damage), measuring volumes' changes with normal development and in hydrocephalic patients, are also reported for demonstration purposes.

Conclusions: The proposed approach allows fully automated segmentation of BP and iCSF in clinical studies, also in severely distorted brains, enabling to assess age- and disease-related changes in intracranial tissue volume with an accuracy comparable to expert manual segmentation.

KEYWORDS

brain parenchyma, intracranial CSF, MRI, pediatric hydrocephalus, segmentation

Carmela Russo and Maria Agnese Pirozzi contributed equally to this study (shared first authorship). Giuseppe Cinalli and Mario Quarantelli contributed equally to this study (shared senior authorship).

This is an open access article under the terms of the [Creative Commons Attribution-NonCommercial-NoDerivs](https://creativecommons.org/licenses/by-nc-nd/4.0/) License, which permits use and distribution in any medium, provided the original work is properly cited, the use is non-commercial and no modifications or adaptations are made.

© 2023 The Authors. *Medical Physics* published by Wiley Periodicals LLC on behalf of American Association of Physicists in Medicine.

1 | INTRODUCTION

Measurements of the volume of the brain parenchyma (BP) and the intracranial cerebrospinal fluid (iCSF) are deemed clinically useful both in the study of typical brain development^{1–6} and for the diagnosis, characterization, and follow-up of pathological conditions in children.^{3,7–12} Several techniques have been devised that allow fully automated and reliable measurement of intracranial brain tissue volumes, including BP and iCSF volumes, in both adult and pediatric patients, through segmentation of MRI studies (for a review see Refs. 13–15). To achieve full automation, these techniques usually rely on an accurate spatial normalization of the MRI studies to a standard template, where probability maps of different tissues are defined a priori. This approach is, however, problematic in neonatal studies, where age-specific templates and tissue probability maps (TPMs) are needed due to the continuous age-related changes in brain size, shape, and signal related to normal development.¹⁶ These limitations, coupled with the lower contrast-to-noise ratio typically encountered in pediatric studies due to the smaller brain size and shorter scan times,¹⁷ as well as to the GM/CSF partial volume effects mimicking the unmyelinated white matter signal,¹⁸ render segmentation of neonatal intracranial tissues particularly challenging.¹⁴ Furthermore, these techniques cannot be successfully applied when severe anatomical alterations are present.¹⁹

As a consequence, pediatric applications of automated MRI segmentation methods have been essentially limited to studying tissue volume changes occurring with normal brain development,^{20,21} or in pathologies that do not display major alterations of the general shape of the brain, such as psychiatric and/or neurodevelopmental brain disorders.²²

In pediatric hydrocephalus, despite the presence of extensive changes in iCSF volume, which render it in principle amenable to successfully perform single-subject analysis for both diagnosis and therapy monitoring, at best semi-automated methods have been validated and applied to dedicated sequences (see Table 1), a setting that does not allow for widespread clinical use.

Nonetheless, a measurement of BP and iCSF volume with a satisfactory degree of accuracy is in principle achievable from clinical routine MRI sequences, considering the high brain CSF-to-parenchyma contrast that is present both in T1-weighted (T1w) and T2-weighted (T2w) sequences, which are routinely acquired in clinical brain MRI studies.

The present study aimed to develop and validate a pipeline for the fully automated measurement of BP, iCSF, and intracranial volume (ICV) in clinical MRI studies (even with different acquisition settings), suitable for use in pediatric hydrocephalic patients, and moreover

without any restrictions in terms of hydrocephalus extent and type. The method exploits, for the first time to the best of our knowledge, the high CSF-to-parenchyma contrast achievable by using T2w to T1w ratio and does not rely on spatial normalization for the CSF and ICV segmentation, so that it is suitable for use in conditions, such as the hydrocephalus, where significant distortions of the brain shape are present.

2 | MATERIALS AND METHODS

2.1 | MRI studies

Reports of the clinical MRI studies from patients undergoing a brain MRI at the Pediatric Neuroradiology Unit of the Santobono-Pausilipon Children's Hospital, Naples, Italy from September 1, 2006 to March 31, 2021 were, retrospectively, analyzed, and those with a diagnosis of hydrocephalus were selected. All studies had been acquired at 1.5 T (Achieva, Philips Medical Systems, The Netherlands) within the routine clinical activity.

Inclusion criteria were the availability of a T2w and a T1w sequence (axial planes covering the whole ICV, sequence parameters selected according to clinical needs, without restricting the analysis to specific sequences and/or sequence parameters), without major artifacts related to patient movements or alterations of the main magnetic field homogeneity due to the presence of ferromagnetic devices.

For the present work, we did not pose any restriction in terms of hydrocephalus type (internal, external, communicating, or obstructive), extent (mono-bi-, tri-, or tetra-ventricular), causes (idiopathic, obstructive, ex vacuo), or of the age of onset (congenital or acquired).

In addition, from the same database, the MRI studies carried out by children from 0 to 168 months of age for clinical conditions not deemed to be associated with brain volume changes (single seizure episode, extracranial vascular angiomas, precocious puberty), once reported as normal by the neuroradiologist, were selected for comparison purposes, and to assess the capacity of the method to measure brain volume modifications with age in the normal population.

Application of the inclusion and exclusion criteria resulted in a database of MRI studies from 66 hydrocephalic patients and 63 controls. Details of all the analyzed subjects are reported in Table 2.

For parameters optimization, we selected from the dataset a subset of nine hydrocephalus studies (ranging from moderate to severe), whereas the method was validated by comparison with results of the manual segmentation in another subset of 23 MRI studies (19 hydrocephalus and four controls).

Analyzed T2w images were all acquired using TurboSpin-Echo sequences (TE ranging between 95

TABLE 1 Literature survey of brain MRI segmentation methods used to assess BP and iCSF volumes in hydrocephalus, where available Dice coefficients are reported along with the main features of the validation datasets.

Reference	Processed sequences	Method	Validation dataset	Dice		
				CSF	BP	ICV
Present study	Clinical	Automated thresholding	4 healthy children and 19 hydrocephalic patients	0.83	0.93	0.96
Grimm et al. ²³	True FISP	CNN	18 hydrocephalic patients	0.81	0.88	—
Radhakrishnan et al. ²⁴	Clinical	Semiautomated region-growing	Brainweb	0.61	0.89	—
Cizmeci et al. ⁷	Clinical	CNN	n/a	—	—	—
Moeskops et al. ²⁵			5, 30wks PMA	0.88–0.91 ^a	—	—
			12, 40wks PMA (LOSO)	0.81–0.86 ^a		
			30, Young adults	0.85–n/a ^a		
			15, Aged adults	0.92–0.76		
Mandell et al. ³	Clinical	Semiautomated edge tracing	Simulated data set	0.62	0.94	—
Grimm et al. ²⁶	True FISP	BET/FAST	15, 65–80 yo, controls	0.70	0.93	0.94
Grimm et al. ²⁷						
Mendrik et al. ²⁸						
St. George et al. ¹²	Clinical	Semiautomated edge tracing	4 healthy children	—	—	—
Jain et al. ¹¹						
Xenos et al. ⁹						
^b Sgouros et al. ⁶						
Vasileiadis et al. ¹⁰	MPRAGE	Semiautomated signal intensity thresholding	n/a	—	—	—

The table shows a summary of brain MRI segmentation studies of pediatric hydrocephalus, where multiple studies are reported, the last one is where the validation data are listed.

^aVentricular-periencephalic CSF.

^bAs validation, only % differences with ICV traced on volumetric sequences were reported (0.06%–4.5%).

Abbreviations: BET, Brain Extraction Tool²⁹; BP, brain parenchyma; CNN, convolutional neural network; CSF, cerebro-spinal fluid; FAST, FMRIB's Automated Segmentation Tool³⁰; ICV, intracranial volume; LOSO, leave-one-subject-out cross-validation; MPRAGE, magnetization-prepared rapid gradient echo; PMA, post-menstrual age (weeks); True FISP, true fast imaging with steady-state precession.

and 200 ms and TR between 442 and 11 000 ms, echo train length between 15 and 38, voxel size between 0.3 and 0.9 mm, slice thickness between 2 and 5 mm).

T1-weighted images were obtained either by 3D Turbo Field-Echo (TE ranging between 3.2 and 4.6 ms and TR between 7.1 and 9.6 ms, flip angle 8°, echo train length between 213 and 232, voxel size between 0.87 and 1 mm, slice thickness 1 mm), 3D Fast Field-Echo (TE 4.6 ms and TR 25 ms, flip angle 30°, voxel size 0.8 mm, slice thickness 1.6 mm with 50% overlap), or Conventional Spin-Echo (TE between 12.5 and 15 ms and TR between 530 and 786 ms, voxel size between 0.49 and 0.9 mm, slice thickness between 3 and 5 mm). Reproducibility of the manual segmentation was assessed in a subset of the validation dataset, including 10 hydrocephalus and four controls.

Finally, to assess the capacity of the method to measure BP and iCSF volume changes with normal development and in hydrocephalic patients, the method has also been applied to the whole dataset.

The study was approved by the Ethics Committee “Cardarelli-Santobono” (Prot. # 00016911—

05/08/2021), who waived the requirement for written informed consent for retrospective data analysis.

2.2 | Manual segmentation

As a reference, for both the optimization of the pipeline parameters and the validation of the procedure, the T2w volumes of a subset of 32 studies (composed of four healthy and 28 hydrocephalic subjects) were manually segmented by a neuroradiologist with more than 20 years of experience (MQ). To this end, CSF and ICV were outlined on the original unprocessed T2w images (and the BP compartment was obtained subtracting CSF voxels from the ICV) using the interactive manual editing routines available in 3D-Slicer (www.slicer.org).³¹ During the annotation process, the neuroradiologist was able to adjust the brightness/contrast settings, if it was needed for better visualization. To assess intrarater reproducibility, the same operator performed in a subset of 14 studies the manual segmentation twice, 1 week apart.

TABLE 2 Details of all the analyzed subjects in the selected dataset for this study.

		Hydrocephalus	Controls
Optimization	Age (mean±SD, Range)	15.9±35.8 (0.1–111.1)	n/a
	Sex (F/M)	3/6	
Validation	Age (mean±SD, Range)	36.7±41.6 (0.6–153.3)	
	Sex (F/M)	5/14	20.5±12.2 (7.7–31.5)
^a Reproducibility	Age (mean±SD, Range)	46.5±49.1 (1–153.3)	2/2
	Sex (F/M)	2/8	
Others	Age (mean±SD, Range)	13.8±15.7 (0–70)	55.8±46 (0–167.6)
	Sex (F/M)	11/27	31/28
Total	Age (mean±SD, Range)	20.7±29.7 (0–153.3)	53.5±45.4 (0–167.6)
	Sex (F/M)	19/47	33/30
	Hydrocephalus type	^b External (<i>n</i> = 22) ^b External + ventriculomegaly (<i>n</i> = 9) ^b Isolated ventriculomegaly (<i>n</i> = 1) ^c Ex vacuo (<i>n</i> = 19) Obstructive triventricular (<i>n</i> = 5) Malformative (<i>n</i> = 9)	<i>n/a</i>

^aTen of the 19 hydrocephalus and the four control studies used for validation were segmented manually twice by the same operator to estimate intra-operator reproducibility of the manual segmentation.

Age is expressed in months.

^bAll patients in the external, external + ventriculomegaly, and isolated ventriculomegaly groups displayed no brain parenchyma signal abnormalities and were negative at the neurological exam at the time of the MRI study.

^cEx vacuo group includes patients with increases in iCSF due to post-hemorrhagic hydrocephalus (*n* = 12, 1 treated by ventriculocisternostomy), evidence of brain atrophy associated with complex malformations (*n* = 2), perinatal hypoxic-ischemic events (*n* = 3), intrauterine CMV, and methylmalonic metabolic encephalopathy (*n* = 1 each).

2.3 | Automated segmentation procedure

The segmentation procedure was written in Matlab (Rel. R2020b; The MathWorks, inc.; Natick, MA, USA), and integrates preprocessing steps from other image-processing software packages.

DICOM files of the selected studies are preliminarily converted to the NIFTI format using the “dcm2nii” conversion routine from the MRICroGL program (<https://www.nitrc.org/projects/mricrogl>).

To ensure the correspondence of the two volumes into a one coordinate system, the T2w volume is then co-registered to the T1w volume into the T1w native space using the intrasubject, intermodality co-registration routine³² implemented in the Statistical Parametric Mapping software (SPM12) with standard parameters for estimation options (normalized mutual information, separation, tolerances, and histogram smoothing). Both volumes are resliced by trilinear interpolation to isometric 0.5 mm × 0.5 mm × 0.5 mm voxel size (1 mm × 1 mm × 1 mm for the optimization steps, see below).

Nonuniformity intensity correction of the MRI images is then applied to both T1w and T2w volumes using the SPM8 method for bias field correction (debiasing), which is based on an objective function that minimizes the entropy of the volume histogram.³³ This preprocessing

step is crucial for volumetric quantification of cerebral tissues to reduce classification error rates during the following segmentation of images into different tissue types.

At this point, the T1w and T2w volumes underwent a full-scale histogram stretch, which was followed by a normalization of the intensity of the voxels in the images.

Subsequently, the two matched isometric volumes undergo a skull-stripping (brain extraction) procedure to zero extracranial voxels. Given the availability in the current setup of two volumes (T1w and T2w) in each study, we chose to use a multiparametric skull-stripping method,³⁴ which combines the information contained in the two acquisitions to obtain a more reliable definition of the inner skull profile, overcoming the limited accuracy of other available deskulling tools in the presence of severe anatomy distortions.³⁵ In the skull-stripping procedure, a weighted average of the T1w and T2w volumes is obtained, assigning to the T1w volume the weight that provides the combined volume with the closest approximation of a practically unimodal symmetric bell-shaped histogram, resulting in a map of relatively uniform signal in both intracranial (including CSF) and extracranial tissues. The bell-shaped histogram of the resulting combined volume is thus approximated to a Gaussian function, and a threshold is automatically calculated. This thresholding consistently provides for

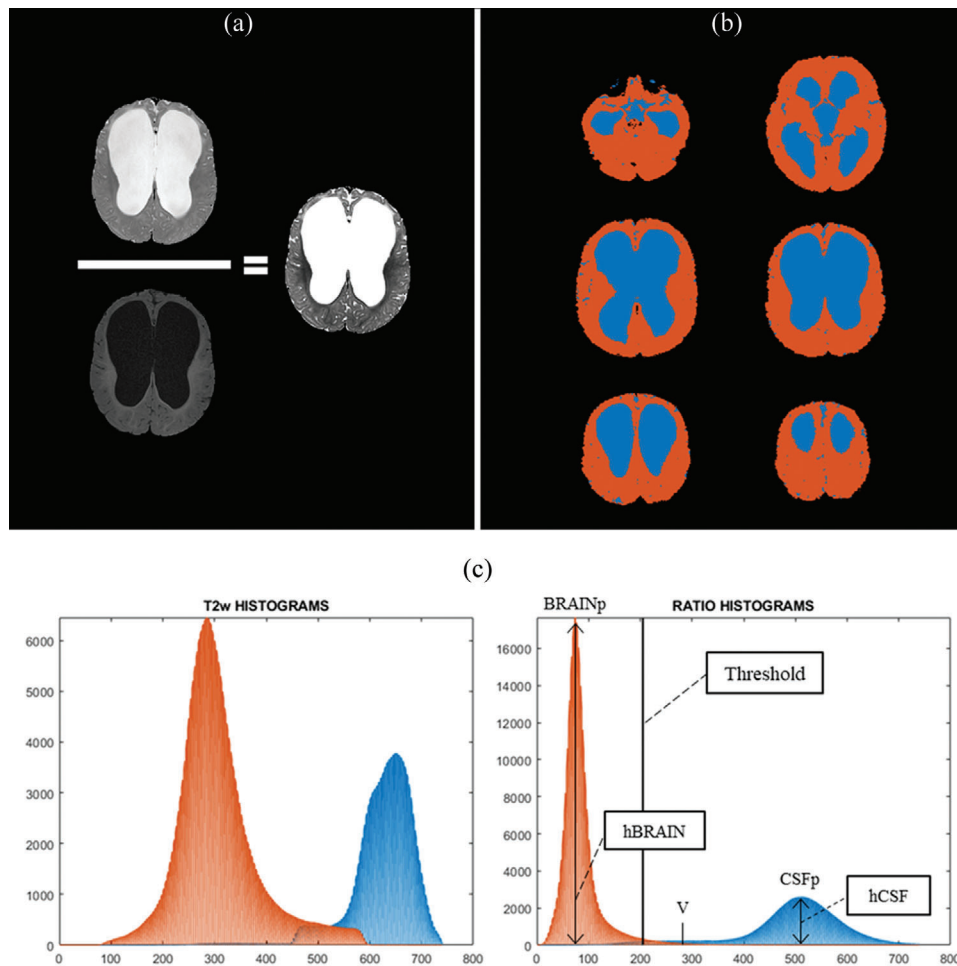


FIGURE 1 T1w and T2w ratio to maximize the CSF-to-parenchyma contrast. (a) To increase the CSF-to-parenchyma contrast, the T2w volume (upper left) is divided by the T1w one (lower left) before subsequent processing. On the right, the resulting ratio image is shown. Increasing in the CSF-to-parenchyma contrast compared to the T2w image can be visually appreciated. For comparison purposes, the three images are scaled so that the mean value of the parenchyma voxels is equal. (b) Selected slices showing the resulting segmentation of the brain parenchyma (in orange) and CSF (in blue) in a triventricular hydrocephalus patient. (c) The corresponding histograms of the manually defined brain (orange) and CSF (blue) voxels are displayed for the original T2-weighted (left), and T2/T1 ratio (right) volumes. A wider separation of the values of the intensities of the voxels of the two tissues can be appreciated, as the brain parenchyma voxels cluster toward lower values, while CSF voxel values are spread toward the upper part of the histogram.

each patient a starting mask where intracranial voxels are almost neatly separated by the peripheral rim of extracranial tissues. A cycle of erosions and dilations is then carried out on the combined volume to further separate the residual extra-cranial voxels from the intracranial ones. The ICV mask is further refined using a conditional expansion, which recover all the CSF voxels at the convexity, which is in turn followed by a regularization of the ICV external surface.³⁴

For subsequent processing, all nonintracranial voxels are zeroed on both the T1w and T2w volumes, which are then combined to maximize the CSF-to-parenchyma contrast. This is achieved by dividing the T2w volume (where CSF has the highest signal intensity among the intracranial tissues) by the T1w volume (where CSF has the lowest signal intensity among the intracranial tissues) (Figure 1).

The intensity histogram of the resulting combined volume, smoothed by a 5-point moving average filter, is analyzed by a peak finding routine, which takes advantage of the a priori knowledge of the possible peak patterns. To this end, peaks with a height smaller than 10% of the maximum of the histogram are disregarded, and a threshold to separate BP from iCSF is defined based on the peak pattern. In particular, in case, a single peak or two peaks differing in height less than 10% are detected, or when the highest peak is the rightmost one (i.e., the histogram patterns in which the CSF and parenchyma peaks are not separated by a valley), the image intensity at a fixed percentage (2.5%) of the peak maximum is used as a threshold, and all intracranial voxels above that value are labeled as CSF. If more than one peak is detected, differing in height more than 10% and/or separated by a valley, the highest one is

considered the parenchyma, and the following formula is used to define the threshold between the parenchyma and CSF peak:

$$\text{Threshold} = \text{BRAIN}_p + F1(\text{CSF}_p - \text{BRAIN}_p) + F2(1 - F1)(V - \text{BRAIN}_p) \left(\frac{h\text{CSF}_p}{h\text{BRAIN}_p} \right)$$

where

- BRAIN_p is the brain parenchyma peak;
- CSF_p is the CSF peak;
- V (valley) is the minimum in the histogram between BRAIN_p and CSF_p ;
- $h\text{CSF}_p$ is the prominence of the CSF peak;
- $h\text{BRAIN}_p$ is the prominence of the parenchyma peak;
- $F1$ is the minimum percentage distance between parenchyma and CSF peak;
- $F2$ is the maximum percentage distance between parenchyma and CSF peak.

The threshold, thus, ranges between a fixed percentage ($F1$) of the distance between the CSF and the parenchyma peak and the valley between the two, in proportion to the relative size of the two peaks (the higher the relative height of the CSF peak, the further from its position the threshold is moved). The optimal $F1$ was found to be 20% on the optimization dataset, whereas the optimal $F2$ was 65%.

Optimization of the parameters of the algorithm (percentage of the peak maximum for single-peak—or others assimilated—distributions, $F1$ and $F2$ in the parenchyma/CSF threshold definition) was obtained separately for each parameter by minimizing the difference between the absolute volumes of CSF obtained by the automated and the manual methods. These iterative optimization steps were carried out using a 1 mm × 1 mm × 1 mm resampling voxel size to allow a reasonable processing time.

2.4 | Statistical analysis

The optimization and validation procedures were done using two separate groups of patients; while the reproducibility of manual segmentation was tested on a subgroup of validation studies (as detailed in Table 2). Then, the proposed method has been applied to the whole dataset of hydrocephalic patient and normal subjects available for demonstration purposes.

iCSF, BP, and ICV obtained by manual and automated segmentation were compared by linear regression and Bland-Altman analyses,³⁶ and their volumetric absolute agreement was assessed using the intraclass correlation coefficient (ICC).³⁷

On the Bland-Altman plots, the presence of a possible correlation between the differences between the manual and automated measures and their means (proportional bias) was also assessed using the Pearson's correlation coefficient.

In addition, the accuracy of the automated method was compared to the intra-operator reproducibility in 14 studies that had been manually assessed twice by the same operator. To this aim, the absolute differences between the two manual measures were compared pairwise with the corresponding ones calculated between their automatic measure and the average of the two manual measures (considered as the gold standard). This comparison was performed to assess whether the differences between the automated method and the mean of the two manual measures were significantly larger than the differences between two manual measures performed by the same operator.

The voxel-by-voxel agreement between the automated and the manual measures was evaluated using the dice similarity coefficient (DSC),³⁸ after obtaining the automatically segmented images in the native T2w space by inversion of the co-registration matrices (see Section 2.3). To this aim, for each of the three metrics (iCSF, BP, and ICV), the volume-weighted averages of the DSC values were calculated both over the entire set of studies used for validation, and on two study subgroups, obtained splitting the validation dataset into low (\leq median value) and high ($>$ median value) volume subgroups, to evaluate the performance of the method as the degree of anatomical distortion increases.

For the validation studies that had been annotated twice, the average volume obtained from the two manual annotations was used for the Bland-Altman analysis, and for the measure of ICCs and DSCs.

The statistical analysis was carried out using the Statistical Package for Social Science (v.16.0, SPSS Inc., Chicago, USA). For all analyses, results were considered significant for $p < 0.05$.

3 | RESULTS

In Figure 2 the results are shown of BP and iCSF segmentation in a control patient (left), in a patient with external hydrocephalus, without overt parenchyma damage (center), and in a patient with post-hemorrhagic hydrocephalus, associated with parenchymal damage (right).

ICCs on the validation set ($n = 23$ subjects, 19 hydrocephalus, and four controls) were 0.984, 0.992, and 0.996 for iCSF, BP, and ICV, respectively, indicating an excellent concordance of the two measures. The corresponding Bland-Altman plots are shown in Figure 3.

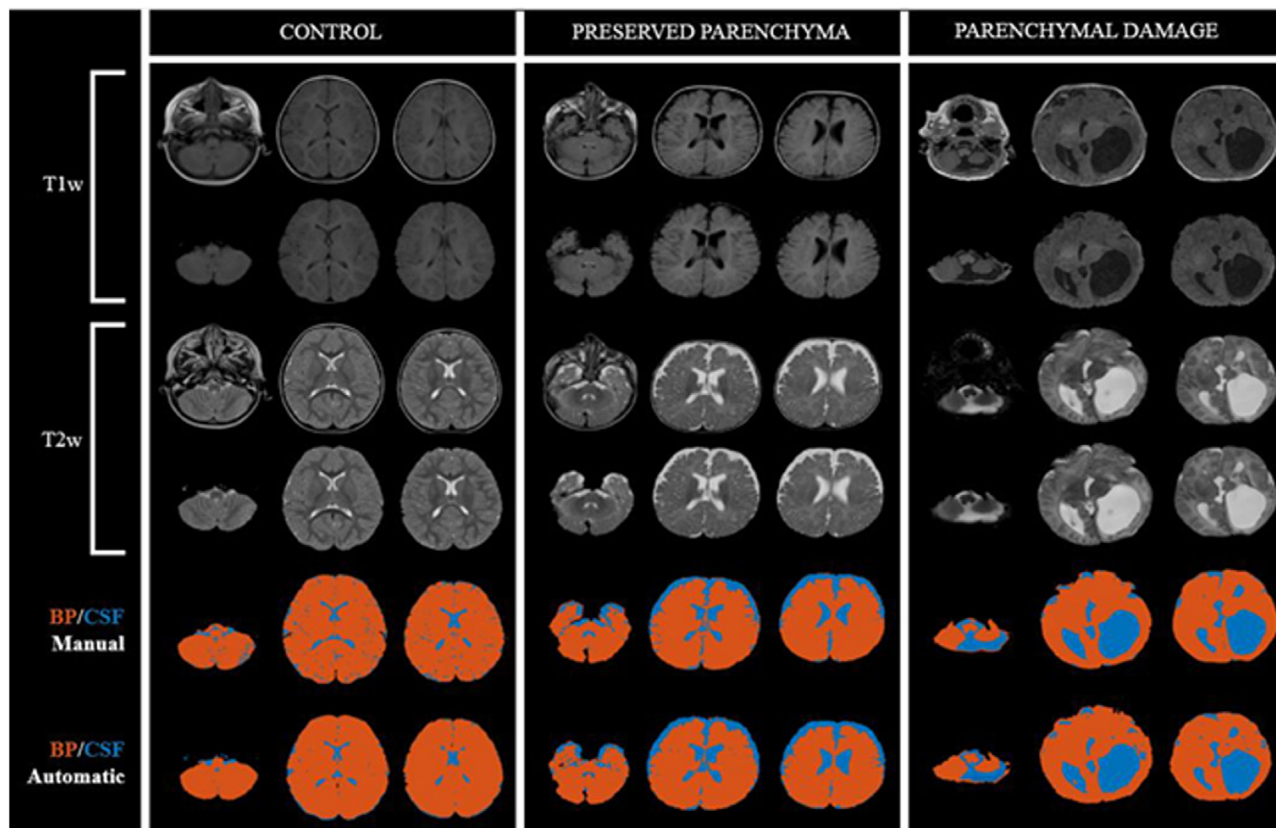


FIGURE 2 Segmentation results in a control patient (left), in a patient with external hydrocephalus (without overt parenchyma damage—central panel), and in a patient with post-hemorrhagic hydrocephalus (associated with parenchymal damage—right panel). For each study, from top to bottom selected planes from the following volumes are reported of T1w volume, deskulled T1w volume, T2w volume, deskulled T2w volume, manually segmented volume, and result of the automated segmentation. In the (manual and automatic) segmented maps, BP voxels are shown in orange and iCSF voxels in blue.

Scatterplots of the automated volumes of BP, iCSF, and ICV, as well as of the CSF/ICV ratio against the corresponding manual measures in both the optimization and validation datasets are shown in Figure 4, along with the corresponding scatterplots of the two manual measures carried out in 14 studies to assess intra-operator reproducibility.

The mean absolute differences between the automatic measures and the average of the two manual measures (reference value) are reported for the three compartments (iCSF, BP, ICV) along with the corresponding mean differences between the two manual measures in Table 3. Manual measures of ICV were highly reproducible (mean absolute difference between the two measures 7.7 ± 6.1 mL), and differences between the automated method and the average of the two manual measures were significantly higher (28.3 ± 21.5 , $p = 0.006$ at paired T -test), although still limited compared to the corresponding mean volumes (on average 2.6% of the ICV). For both BP and iCSF mean absolute differences between the automated method and the average of the two manual measures were smaller than the corresponding differ-

ences between the two manual measures, although nonsignificantly.

Spatial overlap of the automated and manual classifications was excellent, with mean Dice coefficients ranging from 77.2% (for the CSF volumes below the median) to 96.8% for the largest ICVs (Table 4).

Finally, in Figure 5, the volumes of BPF, iCSF, and ICV measured by the method, as well as of CSF/ICV, are plotted versus age for controls ($n = 63$, empty circles), patients with hydrocephalus associated with parenchymal damage ($n = 19$, red dots), and hydrocephalus patients without overt parenchyma damage ($n = 38$, blue dots).

For the present study, the group of preserved BP volume includes, in addition to the patients with external hydrocephalus with and without mild ventriculomegaly (a relatively benign condition associated with increased iCSF spaces), patients with isolated ventriculomegaly, two of the patients with obstructive triventricular hydrocephalus (derived), one patient with Blake's pouch cyst and one with Arnold Chiari II malformation, in whom no parenchymal signal alterations or neurological deficits,

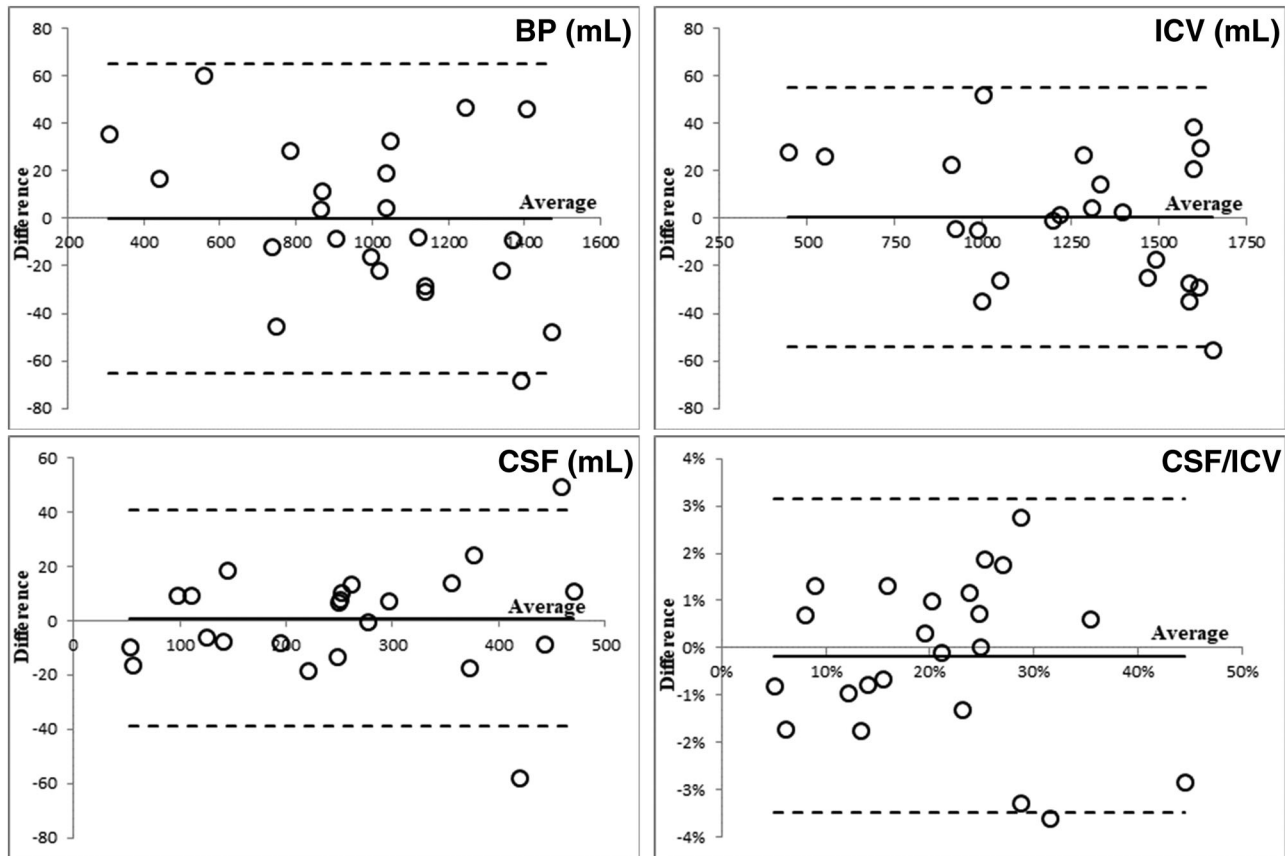


FIGURE 3 Plots of the differences between the automated and manual measures (Y axes), against their means (X axes) according to Bland & Altman.³⁶ Data from the validation dataset are plotted for the brain parenchyma (BP), cerebrospinal fluid (CSF), intracranial volume (ICV), and CSF/ICV measures. For each metric, the mean difference (continuous line) is plotted along with the $\pm 95\%$ confidence interval (dashed lines). No proportional bias emerged from regression analyses for any of the four metrics.

TABLE 3 Absolute average differences between manual measurements and between the average of the two manuals and the automatic one.

	iCSF		BP		ICV	
	[m1–m2]	[auto–man]	[m1–m2]	[auto–man]	[m1–m2]	[auto–man]
Mean	34.7	13.0	36.7	19.4	7.7	20.6
SD	31.0	11.4	31.7	17.2	6.2	14.8
Min	2.4	0.2	0.5	3.9	0.4	1.0
Max	107.7	49.3	104.5	68.4	18.7	55.1
p	0.043		0.144		0.013	

All volumes are expressed in milliliters. For each of the three compartments, estimates of the variability of the manual measures ([m1–m2], the absolute difference between the two measures) are reported, along with the absolute differences between the automated method and the average of the two manual measures ([auto–man]). Mean, standard deviations (SD), and ranges (Min and Max) are reported along with the corresponding *p*-values from the paired *t*-tests.

Abbreviations: BP, Brain parenchyma; CSF, cerebro-spinal fluid; ICV, intracranial volume.

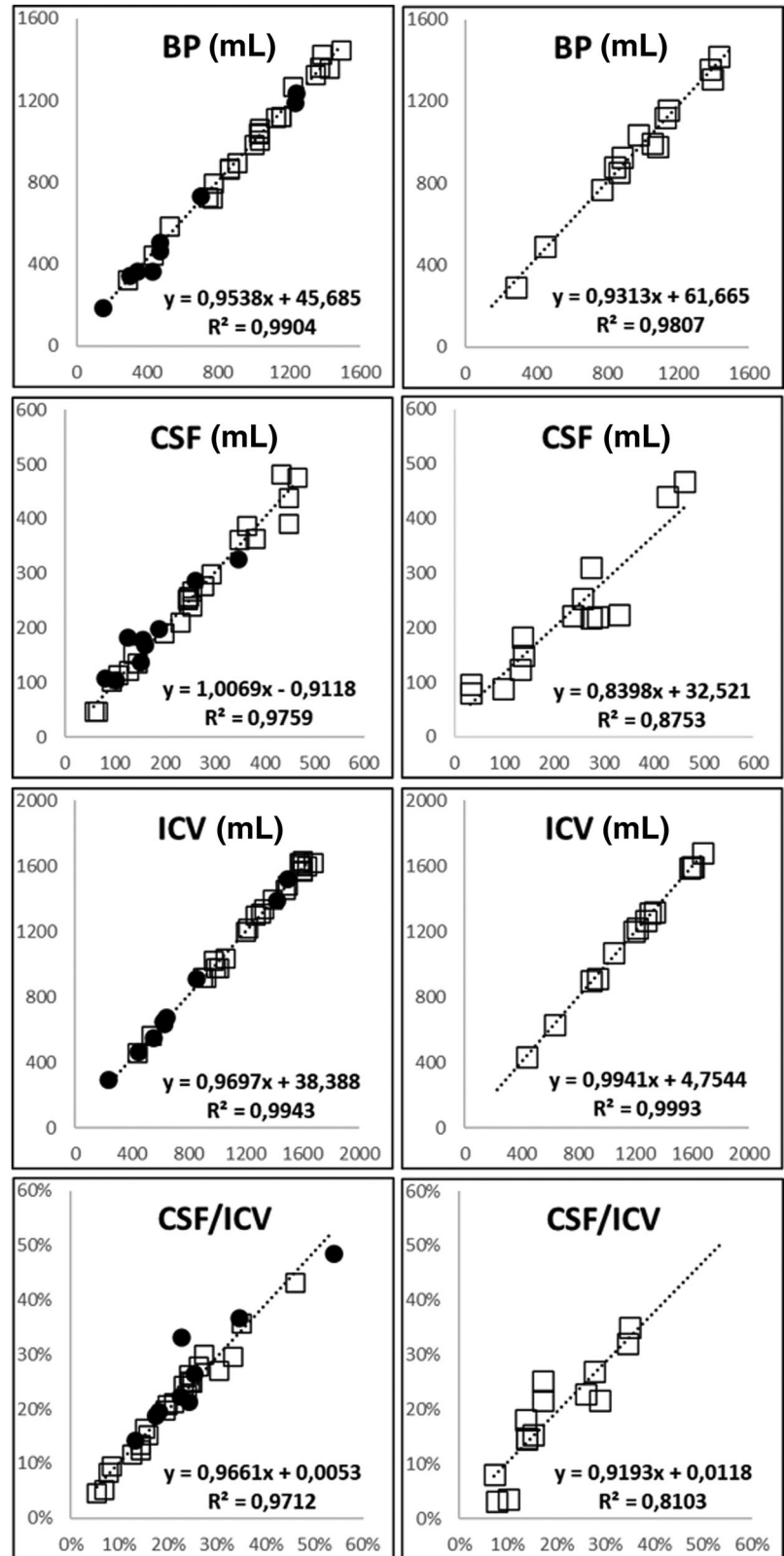
TABLE 4 Dice similarity coefficients for the 23 validation studies.

	iCSF (median = 246.7 mL)			BP (median = 1029.2 mL)			ICV (median = 1308.5 mL)		
	Mean	Min	Max	Mean	Min	Max	Mean	Min	Max
Whole set (n = 23)	84.4%	50.7%	96.4%	93.6%	86.1%	96.8%	97.1%	94.4%	98.6%
≤ Median (n = 12)	78.5%	50.7%	86.8%	92.6%	86.1%	95.4%	96.9%	94.4%	98.6%
> Median (n = 11)	86.7%	76.4%	96.4%	94.2%	89.4%	96.8%	97.2%	95.0%	98.5%

For each metric, results are reported for the whole data set, and for the low (\leq median) and high ($>$ median) volume subgroups.

Abbreviations: BP, brain parenchyma; CSF, cerebro-spinal fluid; ICV, intracranial volume.

FIGURE 4 Scatterplots of automatic versus manual measures to assess intra-operator reproducibility. The first column shows the scatterplots of the brain parenchyma (BP), cerebrospinal fluid (CSF), and intracranial volume (ICV), along with the CSF/ICV ratio, as measured by the automated method versus the manual assessment, for both the optimization (black circles, $n = 9$) and validation (empty squares, $n = 23$) dataset. The regression lines are calculated for the validation dataset. The second column shows the scatterplots of the two manual measures carried out by the same operator in the reproducibility dataset of 14 studies (10 hydrocephalus and four controls).



as reported in the clinical records, were present at the time of the MRI study.

Patients with established parenchymal damage include patients with increases in iCSF due to post-hemorrhagic hydrocephalus ($n = 12$, 1 treated by

ventriculocisternostomy), evidence of brain atrophy associated with complex malformations ($n = 2$), perinatal hypoxic-ischemic events ($n = 3$), intrauterine cytomegalovirus (CMV), and methylmalonic metabolic encephalopathy ($n = 1$ each).

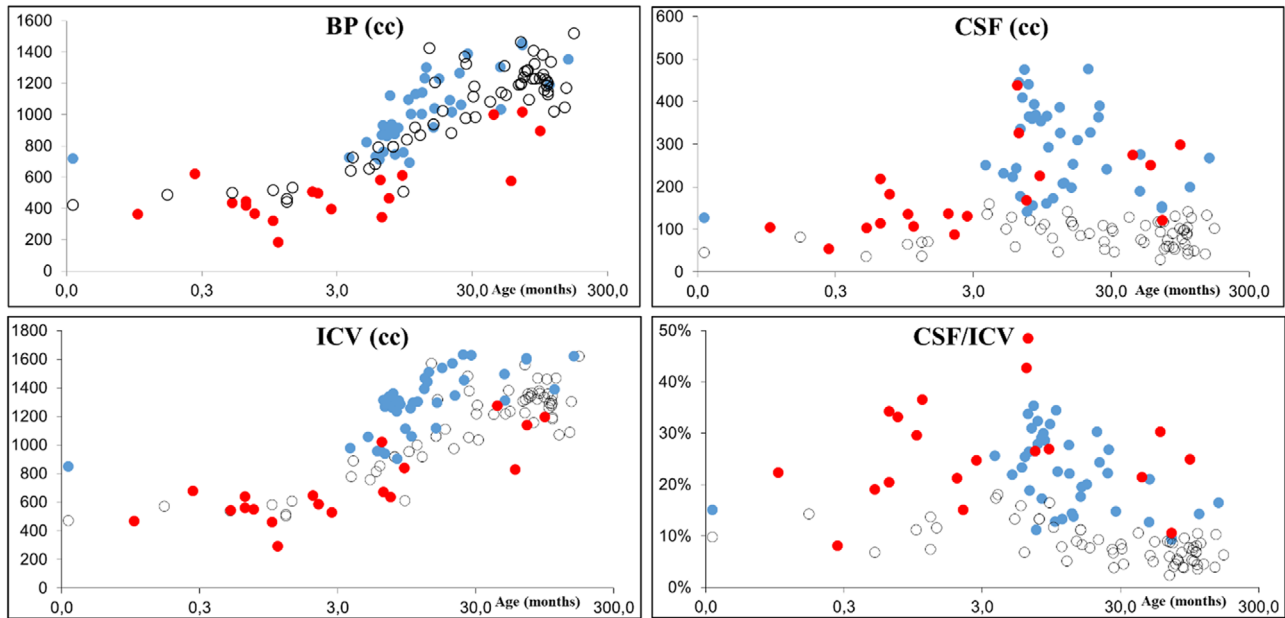


FIGURE 5 Scatterplots of the brain parenchyma (BP), cerebrospinal fluid (CSF), total intracranial volumes (ICV), along with the CSF/ICV ratio versus age of controls ($n = 63$, empty circles), patients with hydrocephalus associated with parenchymal damage ($n = 19$, red dots), and conditions limited to increase in iCSF volume ($n = 38$, blue dots). In patients with increased iCSF volume associated with brain damage, normal or slightly reduced ICV compared to controls can be appreciated, also resulting in an increased CSF/ICV ratio. On the contrary, in patients with hydrocephalus not associated with brain parenchyma damage, BP volumes overlap with those of controls, while CSF and ICV volumes, and consequently the CSF/ICV ratio, are increased.

In patients with increased iCSF volume associated with brain damage, normal or slightly reduced ICV and reduced BP volume compared to controls can be appreciated, also resulting in an increased CSF/ICV ratio. On the other hand, the other hydrocephalus patient group shows BP volumes overlapping with those of controls, while an increase in iCSF can be appreciated, with consequently increased ICV and reduced BP/ICV ratio.

4 | DISCUSSION

We developed a novel method to automatically segment BP and iCSF from couples of T2w and T1w volumes, suitable for the analysis of routine clinical MRI studies of severely distorted brains.

The procedure has been validated against the manual definition of iCSF and BP compartments on T2w datasets, showing an accuracy comparable to the intra-operator reproducibility on a set of studies comprising severe hydrocephalic patients, and results of its application to a sizeable dataset of normal and abnormal studies are presented.

Several previous studies (summarized in Table 1) have adapted segmentation methods originally developed for the adult brain or have applied new approaches based on artificial intelligence to obtain intracranial tissue volume measures from MRI studies of patients with hydrocephalus.

In most cases, these methods, however, have been applied to dedicated volumetric sequences, and none of the methods proposed for processing of clinical studies has been validated against manual measures in pathologic cases, where their accuracy is deemed to drop.

In particular, the “Brain Extraction Tool” (BET²⁹) and the FMRIB’s Automated Segmentation Tool (FAST³⁰) both implemented in the FMRIB Software Library for use in adults, have been recently used jointly to assess hydrocephalus, proving capable of assessing CSF changes after surgical treatment.²³ This approach, however, has been applied to dedicated highly T2w (1-mm isometric 3D true FISP) sequences, and a proper validation against manual assessment was not carried out.

Alternatively, the use of recently introduced relaxometric techniques based on dedicated sequences, such as the “Synthetic MRI” approach based on the QMAP sequence,³⁹ has the potential to render the segmentation process independent of anatomical information, and thus applicable to highly distorted brains. However, the current implementation of the method has provided limited accuracy in segmenting CSF and BP in studies from subjects below 1 year of age.⁴⁰

Other segmentation methods for neonatal and pediatric MRI that have been designed to be relatively independent of anatomical deformations and/or tissue signal intensity changes, lack quantitative validation on

this type of studies, and their validation on healthy controls has provided Dice coefficients for iCSF similar to ours (e.g., 0.84 ± 0.02 for Gui et al.⁴¹).

Our estimates of age-related brain volume changes in normal subjects are in line with previous literature data based on neuroimaging data segmentation. In particular, previous studies using a combination of fully automated and semimanual definitions of ICV on MRI studies [e.g., $157.9 \cdot \log(\text{Age in days}) - 104.1$ in Breakey et al.⁴²], or of CT scans⁴³ have provided results, which are overall comparable with ours.

In addition, we have applied the method to the studies in our dataset from two groups of patients in whom preserved or reduced BP volume, respectively, could be expected based on clinical history and MRI findings. When comparing these two groups to the controls, volumetric estimates provided by the method clearly separated these two populations, consistent with the underlying conditions, suggesting a potential role of these measures in supporting the diagnosis of BP damage.

Whereas the proposed method has the advantage of being relatively independent of sequence parameters, so that it is suitable for the analysis of routine clinical studies, and validation data demonstrate an accuracy comparable or superior to other methods based on dedicated sequences, some limitations should be mentioned here:

- The method in its current implementation does not separate ventricular and peri-encephalic iCSF so that conditions in which one compartment is increased at expense of the other would provide in principle normal results. Similarly, pencephalic cavities are not separately segmented;
- Although no restrictions were imposed on the sequence type, and an ample heterogeneity of sequences was allowed in the dataset used for the study, validation on other scanners is warranted to further rule out the effect of different sequence implementations by different equipment manufacturers, as well as the performance of the method at other field strengths;
- Although manual contouring represents the only possible gold standard for the definition of intracranial compartments in clinical studies, it suffers from obvious accuracy limitations, as exemplified here by the limited intra-operator accuracy (columns [m1–m2] in Table 3 and second column in Figure 4). Alternatively, the use of MRI simulations has been proposed, which has in principle the advantage of providing a proper ground truth (e.g., BrainWeb,⁴⁴ Phantomag⁴⁵). However, this approach has been employed so far only to simulate the adult brain, and currently, no hydrocephalus simulations are available.

5 | CONCLUSIONS

We have developed a tool for fully automated segmentation of iCSF and BP volumes suitable for processing of clinical pediatric MRI scans, which is independent of anatomical information, and is, thus, capable of processing MRI studies from severely distorted brains. The method is fully operator-independent, and no assumptions are made on image contrast other than a generic T1- and T2-weighting of the two sequences used for the analysis, so that it can be applied in principle to practically any clinical dataset. Validation results across a large spectrum of hydrocephalus severities demonstrated accuracy comparable to the one obtained by other currently available segmentation methods on MRI studies from healthy controls, and comparable to the intra-operator reproducibility of manual segmentation, allowing to study both age- and pathology-related intracranial tissue volume changes.

The proposed fully automated segmentation method is based on the use of T2w/T1w ratio as a solid basis for CSF/BP segmentation. This novel approach proved suitable for processing nondedicated, clinical MRI studies from patients with hydrocephalus, as demonstrated by the validation results. The proposed method provides, for the first time to the best of our knowledge, a validated fully automated tool for BP/CSF segmentation, for use in pathologies characterized by severe anatomic distortions, for which no properly validated tool capable of processing clinical sequences was currently available.

CREDIT STATEMENT

Carmela Russo: Methodology; investigation; validation; data curation; writing—original draft. **Maria Agnese Pirozzi:** Methodology; software; validation; writing—original draft. **Federica Mazio:** Investigation; validation; data curation. **Daniele Cascone:** Investigation; validation; data curation. **Domenico Cicala:** Investigation; validation; data curation. **Maria De Liso:** Investigation; validation; data curation. **Anna Nastro:** Investigation; validation; data curation. **Eugenio Maria Covelli:** Conceptualization; investigation; validation; writing—review and editing. **Giuseppe Cinalli:** Conceptualization; writing—review and editing. **Mario Quarantelli:** Conceptualization; methodology; software; validation; writing—review and editing.

ACKNOWLEDGMENTS

The authors have nothing to report.


CONFLICT OF INTEREST STATEMENT

The authors declare no conflicts of interest.


DATA AVAILABILITY STATEMENT

Authors will share data upon request with the corresponding author.

ORCID

Maria Agnese Pirozzi 

<https://orcid.org/0000-0002-4632-3513>

Mario Quarantelli 

<https://orcid.org/0000-0001-7836-454X>

REFERENCES

- Courchesne E, Chisum HJ, Townsend J, et al. Normal brain development and aging: quantitative analysis at in vivo MR imaging in healthy volunteers. *Radiology*. 2000;216(3):672-682. doi:10.1148/RADIOLOGY.216.3.R00AU37672
- Hüppi PS, Warfield S, Kikinis R, et al. Quantitative magnetic resonance imaging of brain development in premature and mature newborns. *Ann Neurol*. 1998;43(2):224-235. doi:10.1002/ANA.410430213
- Mandell JG, Langelaan JW, Webb AG, Schiff SJ. Volumetric brain analysis in neurosurgery: part 1. Particle filter segmentation of brain and cerebrospinal fluid growth dynamics from MRI and CT images. *J Neurosurg Pediatr*. 2015;15(2):113-124. doi:10.3171/2014.9.PEDS12426
- Tamnes CK, Walhovd KB, Dale AM, et al. Brain development and aging: overlapping and unique patterns of change. *Neuroimage*. 2013;68:63-74. doi:10.1016/j.neuroimage.2012.11.039
- Xenos C, Sgouros S, Natarajan K. Ventricular volume change in childhood. *J Neurosurg*. 2002;97(3):584-590. doi:10.3171/JNS.2002.97.3.0584
- Sgouros S, Goldin JH, Hockley AD, Wake MJC, Natarajan K. Intracranial volume change in childhood. *J Neurosurg*. 1999;91(4):610-616. doi:10.3171/jns.1999.91.4.0610
- Cizmeci MN, Khalili N, Claessens NHP, et al. Assessment of brain injury and brain volumes after posthemorrhagic ventricular dilatation: a nested substudy of the Randomized Controlled ELVIS Trial. *J Pediatr*. 2019;208:191-197.e2. doi:10.1016/j.jpeds.2018.12.062
- Fletcher JM, McCauley SR, Brandt ME, et al. Regional brain tissue composition in children with hydrocephalus. Relationships with cognitive development. *Arch Neurol*. 1996;53(6):549-557. doi:10.1001/ARCHNEUR.1996.00550060093022
- Xenos C, Sgouros S, Natarajan K, Walsh AR, Hockley A. Influence of shunt type on ventricular volume changes in children with hydrocephalus. *J Neurosurg*. 2003;98(2):277-283. doi:10.3171/jns.2003.98.2.0277
- Vasileiadis GT, Gelman N, Han VKM, et al. Uncomplicated intraventricular hemorrhage is followed by reduced cortical volume at near-term age. *Pediatrics*. 2004;114(3). doi:10.1542/peds.2004-0500
- Jain H, Natarajan K, Sgouros S. Influence of the shunt type in the difference in reduction of volume between the two lateral ventricles in shunted hydrocephalic children. *Childs Nerv Syst*. 2005;21(7):552-558. doi:10.1007/S00381-004-1096-Y
- St George E, Natarajan K, Sgouros S. Changes in ventricular volume in hydrocephalic children following successful endoscopic third ventriculostomy. *Child's Nerv Syst*. 2004;20(11-12):834-838. doi:10.1007/s00381-004-0939-x
- Li G, Wang L, Yap PT, et al. Computational neuroanatomy of baby brains: a review. *Neuroimage*. 2019;185:906-925. doi:10.1016/j.neuroimage.2018.03.042
- Makropoulos A, Counsell SJ, Rueckert D. A review on automatic fetal and neonatal brain MRI segmentation. *Neuroimage*. 2018;170:231-248. doi:10.1016/j.neuroimage.2017.06.074
- Devi CN, Chandrasekharan A, Sundararaman VK, Alex ZC. Neonatal brain MRI segmentation: a review. *Comput Biol Med*. 2015;64:163-178. doi:10.1016/j.combiomed.2015.06.016
- Işgum I, Benders MJNL, Avants B, et al. Evaluation of automatic neonatal brain segmentation algorithms: the NeoBrainS12 challenge. *Med Image Anal*. 2015;20(1):135-151. doi:10.1016/j.media.2014.11.001
- Prastawa M, Gilmore JH, Lin W, Gerig G. Automatic segmentation of MR images of the developing newborn brain. *Med Image Anal*. 2005;9(5):457-466. doi:10.1016/J.MEDIA.2005.05.007
- Xue H, Srinivasan L, Jiang S, et al. Automatic segmentation and reconstruction of the cortex from neonatal MRI. *Neuroimage*. 2007;38(3):461-477. doi:10.1016/J.NEUROIMAGE.2007.07.030
- Helms G. Segmentation of human brain using structural MRI. *Magn Reson Mater Phys, Biol Med*. 2016;29(2):111-124. doi:10.1007/s10334-015-0518-z
- Levman J, Takahashi E. Multivariate analyses applied to healthy neurodevelopment in fetal, neonatal, and pediatric MRI. *Front Neuroanat*. 2016;9. doi:10.3389/FNANA.2015.00163
- Knickmeyer RC, Gouttard S, Kang C, et al. A structural MRI study of human brain development from birth to 2 years. *J Neurosci*. 2008;28(47):12176-12182. doi:10.1523/JNEUROSCI.3479-08.2008
- Levman J, Takahashi E. Multivariate analyses applied to fetal, neonatal and pediatric MRI of neurodevelopmental disorders. *NeuroImage Clin*. 2015;9:532-544. doi:10.1016/J.NICL.2015.09.017
- Grimm F, Edl F, Kerscher SR, Nieselt K, Gugel I, Schuhmann MU. Semantic segmentation of cerebrospinal fluid and brain volume with a convolutional neural network in pediatric hydrocephalus—transfer learning from existing algorithms. *Acta Neurochir (Wien)*. 2020;162(10):2463-2474. doi:10.1007/s00701-020-04447-x
- Radhakrishnan R, Brown BP, Kralik SF, et al. Frontal occipital and frontal temporal horn ratios: comparison and validation of head ultrasound-derived indexes with MRI and Ventricular volumes in infantile ventriculomegaly. *AJR Am J Roentgenol*. 2019;213(4):925-931. doi:10.2214/AJR.19.21261
- Moeskops P, Viergever MA, Mendrik AM, De Vries LS, Benders MJNL, Išgum I. Automatic segmentation of MR brain images with a convolutional neural network. *IEEE Trans Med Imaging*. 2016;35(5):1252-1261. doi:10.1109/TMI.2016.2548501
- Grimm F, Edl F, Gugel I, Kerscher SR, Schuhmann MU. Planar single plane area determination is a viable substitute for total volume of CSF and brain in childhood hydrocephalus. *Acta Neurochir (Wien)*. 2020;162(5):993-1000. doi:10.1007/s00701-019-04160-4
- Grimm F, Edl F, Gugel I, Kerscher SR, Bender B, Schuhmann MU. Automatic volumetry of cerebrospinal fluid and brain volume in severe paediatric hydrocephalus, implementation and clinical course after intervention. *Acta Neurochir (Wien)*. 2020;162(1):23-30. doi:10.1007/s00701-019-04143-5
- Mendrik AM, Vincken KL, Kuijff HJ, et al. MRBrainS challenge: online evaluation framework for brain image segmentation in 3T MRI scans. *Comput Intell Neurosci*. 2015;2015. doi:10.1155/2015/813696
- Smith SM. Fast robust automated brain extraction. *Hum Brain Mapp*. 2002;17(3):143-155. doi:10.1002/hbm.10062
- Zhang Y, Brady M, Smith S. Segmentation of brain MR images through a hidden Markov random field model and the expectation-maximization algorithm. *IEEE Trans Med Imaging*. 2001;20(1):45-57. doi:10.1109/42.906424
- Fedorov A, Beichel R, Kalpathy-Cramer J, et al. 3D Slicer as an image computing platform for the Quantitative Imaging Network. *Magn Reson Imaging*. 2012;30(9):1323-1341. doi:10.1016/J.MRI.2012.05.001
- Friston KJ, Ashburner J, Frith CD, Poline JB, Heather JD, Frackowiak RSJ. Spatial registration and normalization of images. *Hum Brain Mapp*. 1995;3(3):165-189. doi:10.1002/HBM.460030303
- Ashburner J. Another MRI bias correction approach. Proceedings of the 8th International Conference on Functional Mapping of the Human Brain. *Neuroimage*. 2002;16(2):10255.
- Pirozzi MA, Tranfa M, Tortora M, et al. A polynomial regression-based approach to estimate relaxation rate maps suitable for multiparametric segmentation of clinical brain MRI

- studies in multiple sclerosis. *Comput Methods Programs Biomed.* 2022;223:106957. doi:10.1016/j.cmpb.2022.106957
35. Kalavathi P, Prasath VBS. Methods on skull stripping of MRI head scan images-a review. *J Digit Imaging.* 2016;29(3):365-379. doi:10.1007/S10278-015-9847-8
36. Bland JM, Altman DG. Measuring agreement in method comparison studies. *Stat Methods Med Res.* 1999;8(2):135-160. doi:10.1177/096228029900800204
37. Johnson WD, Koch GG. Intraclass correlation coefficient. *Int Encycl Stat Sci.* Published online 2011:685-687. doi:10.1007/978-3-642-04898-2_309
38. Dice LR. Measures of the amount of ecologic association between species. *Ecology.* 1945;26(3):297-302. doi:10.2307/1932409
39. West J, Warntjes JBM, Lundberg P. Novel whole brain segmentation and volume estimation using quantitative MRI. *Eur Radiol.* 2012;22(5):998-1007. doi:10.1007/S00330-011-2336-7
40. McAllister A, Leach J, West H, Jones B, Zhang B, Serai S. Quantitative synthetic MRI in children: normative intracranial tissue segmentation values during development. *AJNR Am J Neuroradiol.* 2017;38(12):2364-2372. doi:10.3174/AJNR.A5398
41. Gui L, Lisowski R, Faundez T, Hüppi PS, Lazeyras F, Kocher M. Morphology-driven automatic segmentation of MR images of the neonatal brain. *Med Image Anal.* 2012;16(8):1565-1579. doi:10.1016/J.MEDIA.2012.07.006
42. Breakey RWF, Knoops PGM, Borghi A, et al. Intracranial volume and head circumference in children with unoperated syndromic craniosynostosis. *Plast Reconstr Surg.* 2018;142(5):708E-717E. doi:10.1097/PRS.0000000000004843
43. Kamdar MR, Gomez RA, Ascherman JA. Intracranial volumes in a large series of healthy children. *Plast Reconstr Surg.* 2009;124(6):2072-2075. doi:10.1097/PRS.0B013E3181BCEFC4
44. Collins DL, Zijdenbos AP, Kollokian V, et al. Design and construction of a realistic digital brain phantom. *IEEE Trans Med Imaging.* 1998;17(3):463-468. doi:10.1109/42.712135
45. Alfano B, Commerci M, Larobina M, et al. An MRI digital brain phantom for validation of segmentation methods. *Med Image Anal.* 2011;15(3):329-339. doi:10.1016/J.MEDIA.2011.01.004

How to cite this article: Russo C, Pirozzi MA, Mazio F, et al. Fully automated measurement of intracranial CSF and brain parenchyma volumes in pediatric hydrocephalus by segmentation of clinical MRI studies. *Med Phys.* 2023;1-13. <https://doi.org/10.1002/mp.16445>